Monthly Notices
of the
ROYAL ASTRONOMICAL SOCIETY

MNRAS **466,** 2312–2324 (2017) doi:10.1093/mnras/stw3080
Advance Access publication 2016 November 30

Galaxy And Mass Assembly: the 1.4 GHz SFR indicator, SFR–M_* relation and predictions for ASKAP–GAMA

L. J. M. Davies,[1★] M. T. Huynh,[1] A. M. Hopkins,[2] N. Seymour,[3] S. P. Driver,[1,4] A. G. R. Robotham,[1] I. K. Baldry,[5] J. Bland-Hawthorn,[6] N. Bourne,[7] M. N. Bremer,[8] M. J. I. Brown,[9] S. Brough,[2] M. Cluver,[10] M. W. Grootes,[11] M. Jarvis,[12,13] J. Loveday,[14] A. Moffet,[1] M. Owers,[2,15] S. Phillipps,[1] E. Sadler,[6] L. Wang,[16,17] S. Wilkins[14] and A. Wright[1]

[1]*ICRAR, The University of Western Australia, 35 Stirling Highway, Crawley, WA 6009, Australia*
[2]*Australian Astronomical Observatory, PO Box 915, North Ryde, NSW 1670, Australia*
[3]*ICRAR, Curtin University, Bentley, WA 6102, Australia*
[4]*SUPA, School of Physics and Astronomy, University of St Andrews, North Haugh, St Andrews, Fife KY16 9SS, UK*
[5]*Astrophysics Research Institute, Liverpool John Moores University, IC2, Liverpool Science Park, 146 Brownlow Hill, Liverpool L3 5RF, UK*
[6]*Sydney Institute for Astronomy, School of Physics A28, University of Sydney, NSW 2006, Australia*
[7]*Institute for Astronomy, University of Edinburgh, Royal Observatory, Blackford Hill, Edinburgh EH9 3HJ, UK*
[8]*Astrophysics Group, School of Physics, University of Bristol, Tyndall Avenue, Bristol BS8 1TL, UK*
[9]*School of Physics and Astronomy, Monash University, Clayton, Victoria 3800, Australia*
[10]*Department of Physics and Astronomy, University of the Western Cape, Robert Sobukwe Road, Bellville 7535, South Africa*
[11]*ESA/ESTEC, NL-2201 AZ Noordwijk, the Netherlands*
[12]*Astrophysics, University of Oxford, Denys Wilkinson Building, Keble Road, Oxford OX1 3RH, UK*
[13]*Department of Physics, University of the Western Cape, Bellville 7535, South Africa*
[14]*Astronomy Centre, University of Sussex, Falmer, Brighton BN1 9QH, UK*
[15]*Department of Physics and Astronomy, Macquarie University, NSW 2109, Australia*
[16]*SRON Netherlands Institute for Space Research, Landleven 12, NL-9747 AD Groningen, the Netherlands*
[17]*Kapteyn Astronomical Institute, University of Groningen, Postbus 800, NL-9700 AV Groningen, the Netherlands*

Accepted 2016 November 24. Received 2016 November 22; in original form 2016 August 26

ABSTRACT

We present a robust calibration of the 1.4 GHz radio continuum star formation rate (SFR) using a combination of the Galaxy And Mass Assembly (GAMA) survey and the Faint Images of the Radio Sky at Twenty-cm (FIRST) survey. We identify individually detected 1.4 GHz GAMA–FIRST sources and use a late-type, non-active galactic nucleus, volume-limited sample from GAMA to produce stellar mass-selected samples. The latter are then combined to produce FIRST-stacked images. This extends the robust parametrization of the 1.4 GHz–SFR relation to faint luminosities. For both the individually detected galaxies and our stacked samples, we compare 1.4 GHz luminosity to SFRs derived from GAMA to determine a new 1.4 GHz luminosity-to-SFR relation with well-constrained slope and normalization. For the first time, we produce the radio SFR–M_* relation over 2 decades in stellar mass, and find that our new calibration is robust, and produces a SFR–M_* relation which is consistent with all other GAMA SFR methods. Finally, using our new 1.4 GHz luminosity-to-SFR calibration we make predictions for the number of star-forming GAMA sources which are likely to be detected in the upcoming Australian Square Kilometre Array Pathfinder surveys, Evolutionary Map of the Universe and Deep Investigation of Neutral Gas Origins.

Key words: radiation mechanisms: non-thermal – galaxies: evolution – galaxies: star formation – radio continuum: galaxies.

★ E-mail: luke.j.davies@uwa.edu.au

1 INTRODUCTION

The rate at which galaxies are forming new stars (the star formation rate, SFR) is critical to our understanding of the formation of stellar mass in galaxies and the global evolution of baryonic matter in the Universe. However, accurately measuring SFRs is problematic. This is largely due to the fact that common methods for deriving SFR are limited by either dust obscuration (e.g. see Meurer, Heckman & Calzetti 1999) and/or aperture corrections to account for missing flux in fibre-based spectroscopy (e.g. using the Hα emission line to derive SFRs; e.g. Gunawardhana et al. 2013; Hopkins et al. 2013).

A potentially more robust approach is to measure both the ultraviolet (UV) and total infrared (IR) emission simultaneously [UV+TIR or full spectral energy distribution (SED)-derived SFRs; e.g. Bell et al. 2005; Papovich et al. 2007; Barro et al. 2011, probing both the dust obscured and unobscured SFRs. This approach does not require obscuration corrections, as one completely observes the full (direct and reprocessed) emission from young stars. The number of sources with robust UV+TIR measurements, however, has historically been very small, hampering efforts to analyse large samples of galaxies using this method.

Recently great strides have been made in improving techniques to derive robust SFRs for large samples of galaxies (see Davies et al. 2016, hereafter D16). Complex prescriptions for the treatment of obscuration corrections in the UV, such as using radiative transfer (RT) models (Tuffs et al. 2004; Wood et al. 2008; Popescu et al. 2011; Grootes et al. 2013, 2014, 2016; Popescu & Tuffs 2013; D16), have dramatically improved our ability to reduce the scatter in UV-derived SFRs to that of the intrinsic population. Furthermore, samples of UV+TIR detected sources have increased dramatically with the extensive surveys of *Galaxy Evolution Explorer* (*GALEX*; Martin et al. 2005) and *Herschel* (Pilbratt et al. 2010), and improvements to SED modelling, such as MAGPHYS (da Cunha, Charlot & Elbaz 2008) and CIGALE (e.g. Noll et al. 2009), have allowed us to probe statistically robust samples using UV+TIR SFRs (e.g. see Smith et al. 2012; D16).

Despite these improvements, it is also possible to avoid sources of error induced by obscuration corrections and aperture corrections by using a measure of star formation which is unaffected by dust obscuration, integrated over the whole galaxy and probing down to faint levels. The radio continuum is ideally suited to this. It has long been known that there is a tight correlation between far-infrared (FIR) emission and rest-frame 1.4 GHz radio power (e.g. van der Kruit 1971; Helou, Soifer & Rowan-Robinson 1985; Condon 1992; Yun, Reddy & Condon 2001). This relation arises because emission at both wavelengths is connected with ongoing star formation. Emission from star-forming galaxies at 1.4 GHz is dominated by synchrotron radiation arising from relativistic electrons thought to be accelerated by supernovae shocks (e.g. Harwit & Pacini 1975). Given that massive stars dominate both the supernova rate and dust heating, the FIR–radio correlation arises through the same underlying sources producing the emission at both wavelengths. As the supernova rate is intimately linked to the birth of high-mass stars and emission at these wavelengths is unencumbered by dust obscuration, the non-thermal radio luminosity provides a robust and dust-insensitive measure of the current star formation on $\sim$100 Myr time-scales (e.g. see Condon, Cotton & Broderick 2002). Thermal radio emission is also strongly correlated with star formation (e.g. Galvin et al. 2016), but has a different spectral slope to non-thermal emission (e.g. Condon 1992), and in this work we assume that thermal contribution at 1.4 GHz is negligible (as found for the majority of local star-forming galaxies; Rabidoux et al. 2014).

In order to robustly use 1.4 GHz emission to probe dust-unbiased star formation, we require the observed 1.4 GHz radio power to be well calibrated against reliable measures of star formation using other tracers. There are two different approaches to perform such a calibration: (i) using detailed observations of well-studied nearby galaxies in the high signal-to-noise ratio regime, primarily with dedicated observations (e.g. Kennicutt et al. 2009; Kennicutt & Evans 2012; Heesen et al. 2014), and (ii) the statistical approach of identifying multiple faint sources in large area surveys (e.g. Bell 2003; Hopkins et al. 2003). Until recently, the latter approach has relied on SFR tracers that require dust obscuration and/or aperture corrections to calibrate the 1.4 GHz SFR indicator and have been limited to relatively high radio luminosity systems. With the new full SED and well-calibrated SFR measures from surveys such as the Galaxy And Mass Assembly (GAMA; Driver et al. 2011; Liske et al. 2015) as in D16, we can begin to explore the 1.4 GHz SFR indicator without the need for complex corrections and to significantly lower radio luminosities. In this work we utilize the UV+TIR and MAGPHYS-derived SFRs from D16 (these are described briefly in Section 4) to produce a new 1.4 GHz luminosity to SFR calibration and use stacking techniques to extend the 1.4 GHz luminosity–SFR relation to faint luminosities.

Such calibrations will become extremely powerful with the next generation of deep large area radio continuum surveys from the Square Kilometre Array (SKA) and its precursors, such as Australian Square Kilometre Array Pathfinder (ASKAP)-Evolutionary Map of the Universe (EMU; Norris et al. 2011) and MeerKAT-MIGHTEE (Jarvis 2012). In preparation for these future studies, it is essential that we fully exploit existing data sets in order to explore SFRs derived from the 1.4 GHz radio emission. Here, we use the current state-of-the-art large area radio survey, FIRST, in combination with GAMA to investigate the 1.4 GHz SFR indicator and make predictions for a number of GAMA sources that will be detectable with ASKAP. Throughout this paper we use a standard ΛCDM cosmology with $H_0 = 70\,\mathrm{km\,s^{-1}}$ Mpc^{-1}, $\Omega_\Lambda = 0.7$ and $\Omega_\mathrm{M} = 0.3$.

2 DATA

2.1 GAMA

The extended GAMA survey (GAMA II) covers 286 deg^2 to a main survey limit of $r_\mathrm{AB} < 19.8$ mag in three equatorial regions (G09, G12 and G15) and two southern regions (G02 and G23 survey limit of $i_\mathrm{AB} < 19.2$ mag in G23; Liske et al. 2015). The limiting magnitude of GAMA was initially designed to probe all aspects of cosmic structures on 1 kpc–1 Mpc scales spanning all environments and out to a redshift limit of $z \sim 0.4$. The spectroscopic survey was undertaken using the AAOmega fibre-fed spectrograph (Saunders et al. 2004; Sharp et al. 2006) in conjunction with the Two-degree Field (2dF; Lewis et al. 2002) positioner on the Anglo-Australian Telescope and obtained redshifts for $\sim$280 000 targets covering $0 < z \lesssim 0.5$ with a median redshift of $z \sim 0.2$, and highly uniform spatial completeness (see Baldry et al. 2010; Robotham et al. 2010; Driver et al. 2011, for summaries of GAMA observations).

Full details of the GAMA survey can be found in Hopkins et al. (2013), Driver et al. (2011, 2016a) and Liske et al. (2015). In this work we use the data obtained in the three equatorial regions, which we refer to here as GAMA II$_\mathrm{Eq}$. Stellar masses for the GAMA II$_\mathrm{Eq}$ sample are derived from the *ugriZYJHK* photometry using a method similar to that outlined in Taylor et al. (2011) assuming a Chabrier initial mass function (IMF; Chabrier 2003). Fig. 1 displays the

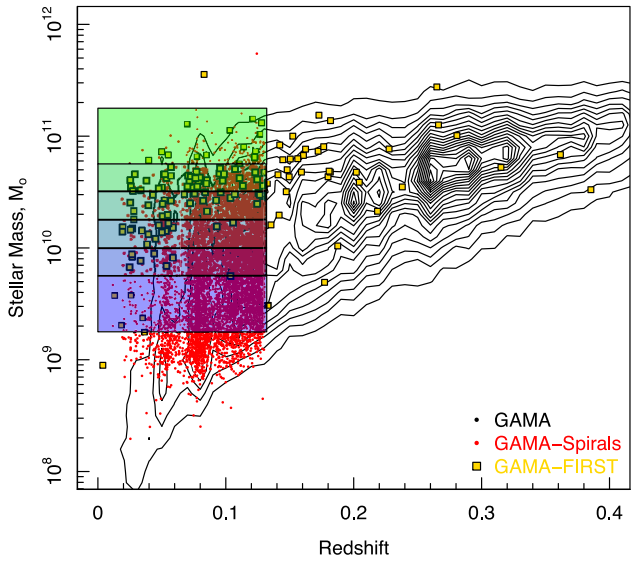

Figure 1. The redshift–M_* distribution of GAMA $\mathrm{II_{Eq}}$ galaxies (contours), the GAMA volume-limited spirals sample of Grootes et al. (2014) used in our stacking analysis (red circles) and the final star-forming GAMA–FIRST sample, excluding all potential AGN sources (gold squares). The coloured shaded regions display the volume stacked within carefully designed stellar mass bins.

stellar mass–redshift distribution of the GAMA $\mathrm{II_{Eq}}$ sample. All photometry used in this work comes from the LAMBDAR catalogue discussed in Wright et al. (2016) and spectral line analysis will be detailed in Gordon et al. (2017).

2.2 FIRST

The Faint Images of the Radio Sky at Twenty-cm (FIRST) survey (Becker, White & Helfand 1995) is a 1.4 GHz continuum survey in the Northern hemisphere and contains ∼90 sources deg^{-2} at the 1 mJy survey threshold to an rms sensitivity of ∼0.15 mJy beam^{-1}. The survey was undertaken by the Very Large Array (VLA) in B configuration with a synthesized restoring beam of 5.4 arcsec full width at half-maximum. We use the '14Dec17' FIRST catalogue which contains observations from 1993 to 2011. This catalogue consists of 946 432 sources covering ∼10 500 deg^2 (i.e. ∼95 deg^{-2}).

3 COMBINING GAMA AND FIRST

3.1 GAMA–FIRST detected sample

To identify GAMA galaxies which have a detection in FIRST, we perform a 3 arcsec cross-match (comparable to the FIRST half beam width, see similar cross-matching in e.g. Sadler et al. 2007) between the GAMA $\mathrm{II_{Eq}}$ galaxies with robust redshifts and photometric measurements, and the FIRST catalogues. Where multiple GAMA sources are matched to a single FIRST detection (<2 per cent of sources), we assign the closest position match. This results in 1991 matched galaxies in the GAMA volume, which we refer to as the GAMA–FIRST sample. We highlight that this sample is comparable to the sample obtained by Ching et al. (2017) who perform a more complex match between Sloan Digital Sky Survey (SDSS) and FIRST galaxies in the GAMA regions.

A substantial fraction of our GAMA–FIRST sources are likely to be active galactic nuclei (AGN) which dominate the 1.4 GHz number counts at high flux density limits. Given that we aim to produce a robust calibration between radio emission and star formation, we opt to exclude all sources which potentially have some fraction of their radio emission arising from an AGN and apply multiple cuts to produce a robust, but by design, incomplete sample of star-forming radio galaxies. 1.4 GHz luminosities for the GAMA–FIRST sample are calculated using the total integrated flux densities (FINT) from the FIRST catalogue, converted to intrinsic luminosity using the GAMA redshifts and k-corrected assuming a power-law slope of $S_\nu \propto \nu^{-0.7}$ (assuming emission from optically thin synchrotron radiation). For completeness, we also perform our analysis assuming an $S_\nu \propto \nu^{-0.6}$ and $S_\nu \propto \nu^{-0.8}$ slope and find that it does not significantly change our results. To remove potential AGN-like sources, we apply the following steps.

(i) First, we exclude sources which are identified as AGN using the BPT diagnostic (Baldwin, Phillips & Terlevich 1981). We select all GAMA–FIRST galaxies which have [O III], Hβ, [N II] and Hα lines detected at $>2\sigma$. The top left-hand panel of Fig. 2 displays the distribution of these sources in the BPT diagram. We use the AGN–SF dividing line of Kauffmann et al. (2003), to exclude sources which are identified as AGN via their optical emission line ratios (i.e. we remove all black points in Fig. 2 from our sample). This removes 236 optically identified AGN.

(ii) This process does not account for heavily obscured (optically thick) AGN, which may not be identified via the BPT method but can still show strong radio emission. In order to remove such sources, we apply the *Wide-field Infrared Survey Explorer* (*WISE*) colour selection of obscured AGN in a similar manner to, for example, Stern et al. (2012) and Mateos et al. (2013). Fig. 2 highlights this. The top right-hand panel of Fig. 2 shows the *WISE* colours for all GAMA sources (contours) and our GAMA–FIRST matched sample (gold). Here we apply a conservative (more strict than previous works) selection of W1 − W2 < 0.125, where W1 and W2 are the observed magnitudes in *WISE*-1 (3.4 μm) and *WISE*-2 (4.6 μm) bands, respectively, taken from the GAMA LAMBDAR catalogue (removing 70 sources).

(iii) We also remove sources which have *WISE* colours consistent with passive galaxies (as their radio emission is likely to arise from an AGN not SF), using the colours of passive spirals outlined in Fraser-McKelvie et al. (2016), W3 − W2 > −0.5, where W3 are the observed magnitudes in *WISE*-3 (12 μm). This removes a further 1277 sources. None of the sources removed here are identified as star forming using the BPT diagnostic as they do not have the required BPT emission lines.

(iv) We then exclude any source which has a rest-frame 1.4 GHz luminosity of $>10^{23.5}$ W Hz^{-1}, as such high luminosities may be representative of an AGN (this luminosity would imply SFR > 200 M$_\odot$ yr^{-1} using previous calibrations), and also sources with exceedingly large 1.4 GHz luminosity in comparison to their measured UV+TIR SFR, excluding sources with $\log_{10}[L_{1.4}] > \log_{10}[\mathrm{SFR}] + 23$ (displayed as the grey shaded region in Fig. 3). This selection may remove ultraluminous infrared galaxies (ULIRGS) which potentially have all of their emission arising from star formation. These sources generally reside at higher redshifts than the GAMA sample however, and thus their potential removal will not affect our derived calibrations. This selection removes a further 170 sources.

(v) In the bottom left-hand panel of Fig. 2, we exclude remaining sources which meet the radio–near-IR (NIR)/mid-IR (MIR) AGN

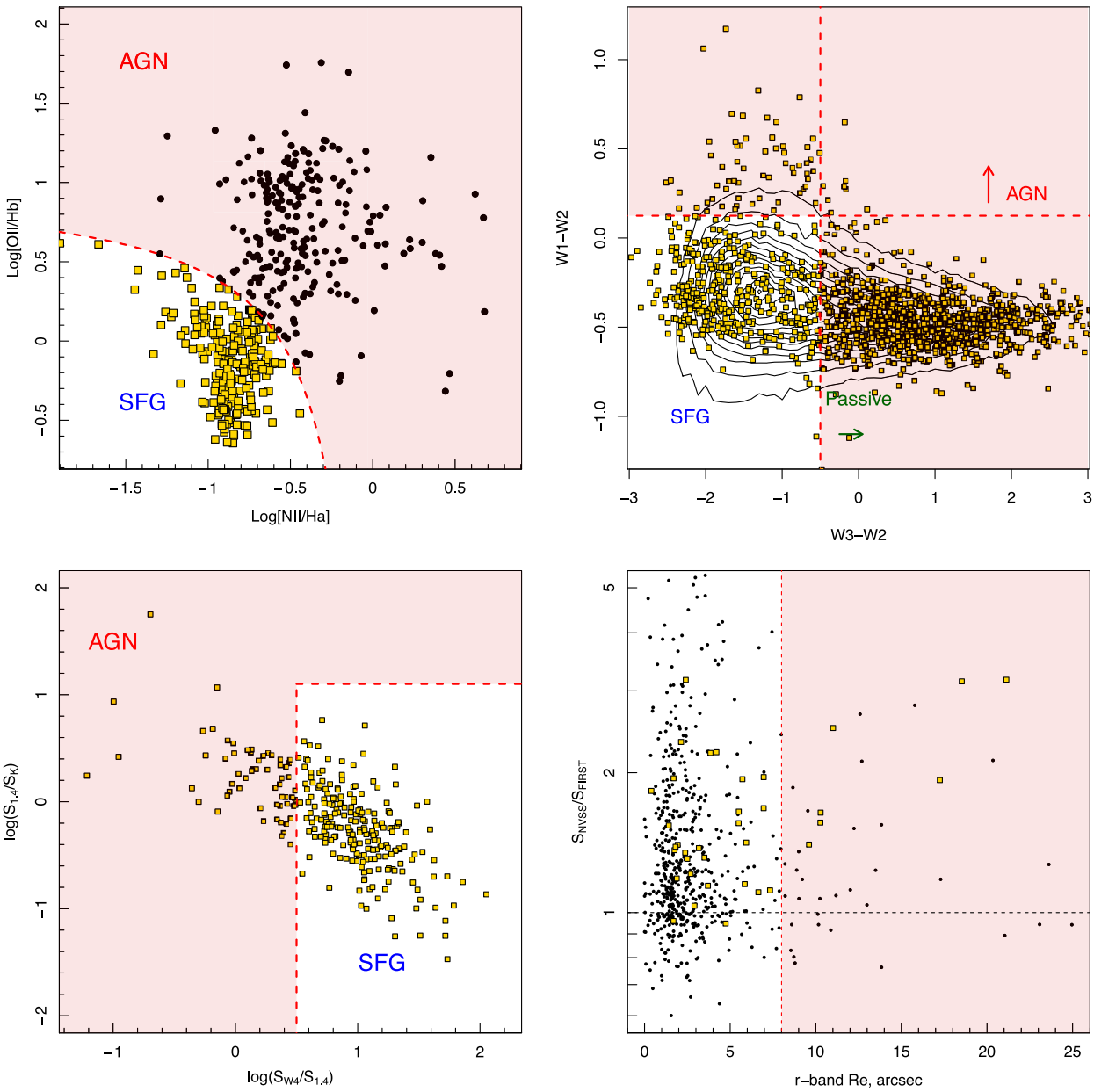

Figure 2. Identification of star-forming galaxies in GAMA–FIRST sample, regions where sources are excluded in our sample selection are shaded red. Top left: BPT classification used to select star-forming galaxies from the GAMA–FIRST cross-matched sample. Points display GAMA–FIRST matched sources which are detected at $>2\sigma$ in all emission lines required for the BPT. The red dashed line displays the SF–AGN dividing line of Kauffmann et al. (2003). We exclude GAMA–FIRST matched sources that are identified as spectroscopic-AGN via the BPT diagram (black points). Gold points remain in our sample. Top right: *WISE* colour selection of obscured AGN sources. Contours display the GAMA sample, while gold squares display the remaining GAMA–FIRST sample, after BPT rejection of AGN. We apply a conservative cut in W3 − W2 $<$ 0.125, red horizontal line, to exclude GAMA–FIRST sources which potentially contain an obscured AGN and also exclude source with W3 − W2 $>$ −0.5, red vertical line, as such systems have colours consistent with passive galaxies (and as such their radio emission is unlikely to arise from star formation. Bottom left: W4/1.4 GHz and 1.4 GHz/*K*-band AGN selection of Seymour et al. (2008). Gold points show sources that remain in our selection after both the BPT and *WISE* selection. Bottom right: The NVSS/FIRST 1.4 GHz flux density ratio as a function of *r*-band effective radius (R_e). Gold points display sources which are still in our selection after all previous cuts, while black points display all sources which are detected in both FIRST and NVSS. Note that not all of the remaining same is shown in this panel as only a subsample has NVSS detections. We exclude all sources with R_e $>$5 arcsec which potentially have resolved out flux in FIRST.

selection of Seymour et al. (2008). We use a conservative selection to exclude as AGN the 115 sources with $\log[S_{22\,\mu m}/S_{1.4\,GHz}] < 0.5$ (where $S_{22\,\mu m}$ is the LAMBDAR *WISE*-4 (22 μm) flux). This may lead to the removal of low-metallicity dwarf galaxies, but this is unlikely to significantly affect our sample.

This leaves 172 non-AGN star-forming galaxies in the GAMA–FIRST sample. Using the high-resolution FIRST data however, also leads to the possibility of radio flux being 'resolved out' for large angular size sources with faint radio emission in their extremities (i.e. Jarvis et al. 2010). This could potentially lead to an underestimation

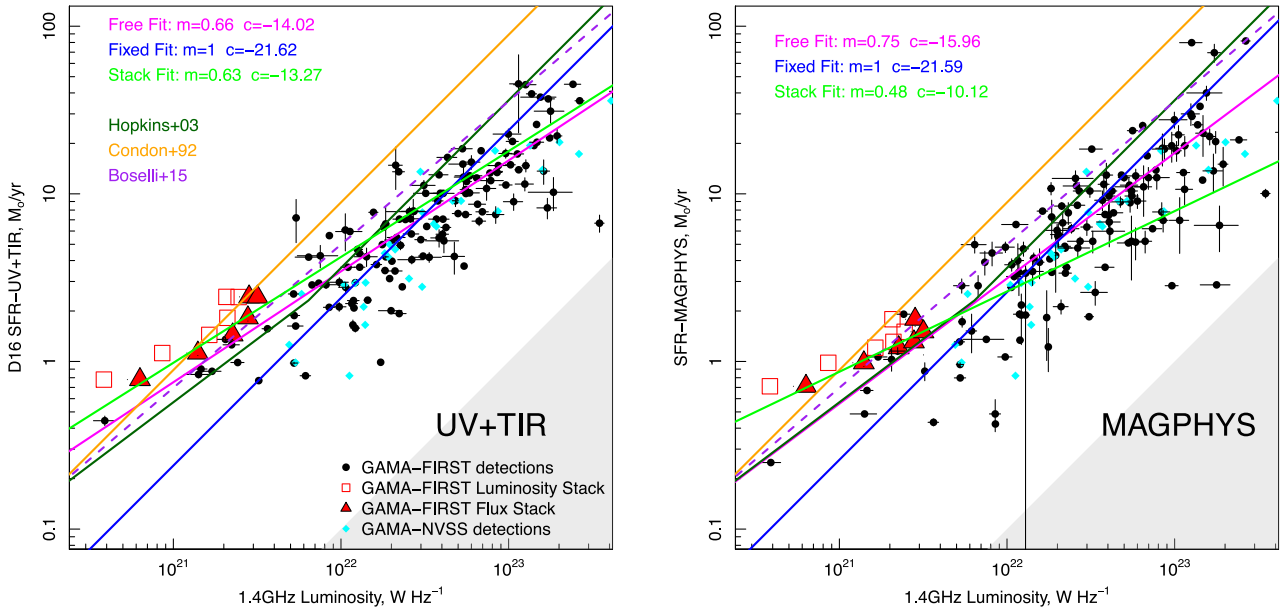

Figure 3. Correlation between 1.4 GHz luminosity and SFR indicators from GAMA outlined in Davies et al. (2016): UV+total IR derived SFR (left) and MAGPHYS SED-derived SFR (right). Circles display the GAMA–FIRST detected sample. Open squares display our luminosity-stacked samples, while filled triangles display our flux density-stacked samples – where errors are smaller than the plotted points. We fit the relations using HYPERFIT for both a free slope and normalization (magenta lines), a fixed $m = 1$ relation (blue lines), a free fit to just the flux density-measured stacked data points (green line). We show the Hopkins et al. (2003), Condon (1992) and Boselli et al. (2015) relations as the dark green, orange and purple dashed lines, respectively. For completeness, we also show the small number of sources in our sample with NVSS detections (cyan diamonds) to highlight that including potential 'resolved-out' flux in our sample would not significantly change our derived relations. Grey shaded region displays where sources with erroneously high 1.4 GHz luminosity are excluded. The excluded points fall off this figure and the grey shaded region is only intended to show that we are not biasing our fits by excluding objects in this region.

of source flux density and thus bias any derived calibrations. In order to investigate this, we use the NRAO VLA Sky Survey (NVSS; Condon et al. 1998), a 1.4 GHz survey using the VLA in the more compact D configuration. This compact configuration has poorer resolution than FIRST but greater sensitivity to extended outlying structure. As such, NVSS provides a robust measurement of total 1.4 GHz flux density, but is more likely to be affected by source confusion. To estimate the fraction of flux that is potentially resolved out, we match to the NVSS catalogue and find that 54 sources in our remaining sample have NVSS detections. Fig. 2 (bottom right) displays the NVSS to FIRST flux density ratio against r-band effective radius taken from GAMA. We display both our robust SF sample (gold squares) and all other FIRST–NVSS matches from our initial 1991 sources (black points). Clearly, NVSS measures a larger 1.4 GHz flux density than FIRST for many sources, but typically finding differences of less than a factor of 2. Here we opt to exclude large sources that are most likely to be affected missing flux in FIRST. We do not exclude sources based on their NVSS to FIRST flux density ratio as not all sources have NVSS detections.

(vi) In a similar manner to Hopkins et al. (2003) but with a more conservative cut, we exclude all sources from our sample with r-band effective radius >8 arcsec, removing a further 24 galaxies. In Fig. 3, displaying our 1.4 GHz luminosity to SFR relation, we show NVSS measurements for our final sample as cyan points, and highlight that the addition of 'resolved out' flux would not strongly affect our derived relations.

(vii) Last, we then visually inspect all remaining sources for broad Hα line emission (potentially broad-line AGN) and/or extended and two-component radio emission (potentially lobed radio galaxies), and exclude a further four systems.

This leaves a final, highly robust, non-AGN star-forming GAMA–FIRST sample of just 144 galaxies. While this sample is small, we have made every possible effort to exclude any sources of AGN contribution to the radio emission. We present the final GAMA–FIRST sample as the gold squares in Fig. 1. This sample largely consists of sources with high radio luminosities and star formation rates (as they are individually detected in the relatively shallow FIRST data). To push to lower radio powers requires the stacking of well-defined populations.

3.2 GAMA–FIRST stacking

To supplement the individually detected GAMA–FIRST galaxies described above, we also perform a stacking analysis of stellar-mass-selected star-forming galaxies within a volume-limited sample from GAMA.

We use the low contamination and high completeness, volume-limited sample of spiral galaxies outlined in Grootes et al. (2016) and D16, and selected following the method presented in Grootes et al. (2014) – hereafter GAMA–SPIRALS. Briefly, the sample uses a non-parametric, cell-based, morphological classification algorithm to identify spiral galaxies at $0 < z < 0.13$. The morphological proxy parameters used in Grootes et al. are the r-band effective radius, i-band luminosity and single-Sérsic index (taken from Kelvin et al. 2012), importantly avoiding observables which are themselves SFR indicators. We refer the reader to Grootes et al. (2014) and Grootes et al. (2016) for further details.

The red points in Fig. 1 display the GAMA–SPIRALS sample, which contains 6366 sources. We then also exclude galaxies which are identified as AGN using the BPT diagnostic, leaving 6149

Table 1. Properties of the GAMA–FIRST stacked samples. Column 1: the stellar mass range over which our volume-limited sample of spiral galaxies is stacked. Column 2: the median redshift of the stacked sample. Column 3: the number of sources in the stacked sample. Column 4: the number of individually detected (peak flux density >0.9 mJy) sources in the stack. Column 5: stacked flux density measurement for all sources. Column 6: stacked flux density measurement excluding individually detected sources. Column 7: luminosity measurement from flux density-measured stack, using stacked flux density and median redshift. Column 8: luminosity measurement from luminosity-measured stack, using individual source redshifts. Luminosity measurements are derived from the full stacks only (not excluding detections), but the error range incorporates the difference between the full stack and the stack with detected sources removed.

Stellar mass $\log[M_*/\mathrm{M}_\odot]$ (1)	Median redshift (2)	# full (3)	# detected (4)	$S_{1.4}$ – full μJy ± rms (5)	$S_{1.4}$ – no detect μJy ± rms (6)	$L_{\text{flux-measured}}$ $\times 10^{21}$ W Hz^{-1} (7)	$L_{\text{lum-measured}}$ $\times 10^{21}$ W Hz^{-1} (8)
9.25–9.75	0.100	2261	7	24.2 ± 5.6	24.2 ± 5.5	0.60 ± 0.14	0.39 ± 0.07
9.75–10.00	0.107	706	4	46.3 ± 9.6	43.5 ± 9.7	1.33 ± 0.38	0.85 ± 0.20
10.00–10.25	0.106	565	1	76.3 ± 11.1	76.3 ± 11.2	2.14 ± 0.31	1.64 ± 0.22
10.25–10.50	0.106	456	3	94.1 ± 12.0	93.4 ± 12.0	2.63 ± 0.34	2.11 ± 0.22
10.50–10.75	0.108	213	6	91.8 ± 17.2	86.0 ± 17.5	2.67 ± 0.67	2.37 ± 0.64
10.75–11.25	0.111	126	5	100.0 ± 23.6	97.0 ± 23.7	2.98 ± 0.70	2.45 ± 0.48

sources. This process may still retain heavily obscured AGN, which are problematic to remove from the sample prior to stacking. If included, such sources could potentially cause a slight overestimation in the stacked 1.4 GHz measurements. We do not exclude galaxies that would be identified as AGN using the *WISE* colour selection in Section 3.1 as we wish to keep our GAMA–SPIRALS sample identical to that used in D16, but note that only 21 (<0.5 per cent) sources in our sample would meet such a selection.

We split the resulting sample into six stellar mass bins in the range $9.25 < \log[M_*/\mathrm{M}_\odot] < 11.25$. We include four intermediate-mass bins of $\Delta\log[M_*/\mathrm{M}_\odot] = 0.25$, bounded by two larger $\Delta\log[M_*/\mathrm{M}_\odot] = 0.5$ bins at the high- and low-mass end to increase signal-to-noise ratio in the resultant stacks where either sources are radio faint (the low-mass end) or the number density of galaxies is low (the high-mass end). Our stacked volumes are displayed as the coloured shaded regions in Fig. 1. Stellar mass ranges, median redshifts and number densities of the stacked samples can be found in Table 1.

We perform the stacking analysis using two different modes both stacking the FIRST data directly, not catalogue measurements. In both modes we apply median stacking to exclude outlying pixels without the need to apply arbitrary cut-offs to the distribution. Median stacking has been found to work successfully when investigating faint sources in FIRST, for example White et al. (2007).

First, we produce stacks by median combining the pixel values of the FIRST data centred on the positions of the GAMA–SPIRAL samples in each mass bin. We then measure the total integrated flux density at the central beam of the median stack using the MIRIAD MAXFIT function and derive a 1.4 GHz luminosity using the median redshift of all sources in the mass bin and *k*-correcting assuming a power-law slope of $\alpha = -0.7$ (median redshifts are given in the second column of Table 1). Hereafter, we will refer to this as the flux density-measured stack. This stacking process essentially assumes that there is no evolution over the redshift range of our sample and that sources are evenly distributed over the redshift range probed.

Secondly, we determine the individual luminosity of the FIRST data at the position of each of the GAMA–SPIRAL samples. For this we extract a region of the FIRST data centred on the position of the GAMA–SPIRALS source, then convert every pixel value into a luminosity at the source's redshift (again assuming $\alpha = -0.7$). We then median combine the pixel values in each extracted region and again measure the total integrated luminosity at the central beam. Hereafter, we will refer to this as the luminosity-measured stack. This stacked sample uses all distance measurements for individual sources, and hence avoids the assumption of no evolution and even distribution over the redshift range.

For each stellar mass range, we also produce identical stacked samples with the individually detected sources removed. In Table 1 we display the median flux density stack measurements for both the full stacks and the stacks with individually detected sources removed. We also display luminosity measurements for both the flux density-measured and luminosity-measured stacks using the full sample. In order to estimate rms errors, we stack the same number of sources as in each stellar mass bin, but at random offset positions in the FIRST data and measure the resultant rms. For the luminosity-measured stack, we calculate the luminosity of all pixels in the offset position using a unique redshift from the GAMA–SPIRALS sample (thus replicating the same redshift distribution in our rms measurements). We do not display luminosity measurements using the stacked sample with individually detected sources removed, but highlight that these only marginally differ from the full-stacked sample (<5 per cent). We also include the difference between the full sample and a sample excluding detected sources in our luminosity errors.

In order to avoid including radio emission from sources outside of the GAMA–SPIRALS sample, or repeat stacking within the sample, we confirm that none of our GAMA–SPIRALS sample overlaps with another GAMA source within 5 arcsec, and thus the FIRST beam size. As such, we do not have to exclude potentially confused sources. However, this does not rule out contributions to the emission arising from sources below the GAMA *r*-band selection limit (these sources are likely to be faint in radio emission) or high-redshift sources which sit within the beam of the GAMA galaxy. Given it is impossible to remove such sources (as there are no deeper spectroscopic observations in the GAMA regions), we cannot make assessments regarding their contribution to the observed flux density. However, given that the results in the following sections display consistency between our stacked samples and individually detected sources, it is unlikely that such faint galaxies strongly contribute to our derived flux densities. We also do not exclude sources which have *r*-band effective radius >8 arcsec in our stacked samples, as in the individual detections. While these sources may potentially have 'resolved out' flux, we wish to keep the stacked sample identical to that used in D10, and note that an *r*-band effective radius <8 arcsec cut would only remove 35 sources (∼1 per cent) from our GAMA–SPIRALS sample.

Fig. 4 displays the full-stacked GAMA–SPIRAL samples in different stellar mass bins. All stacked values include a multiplication

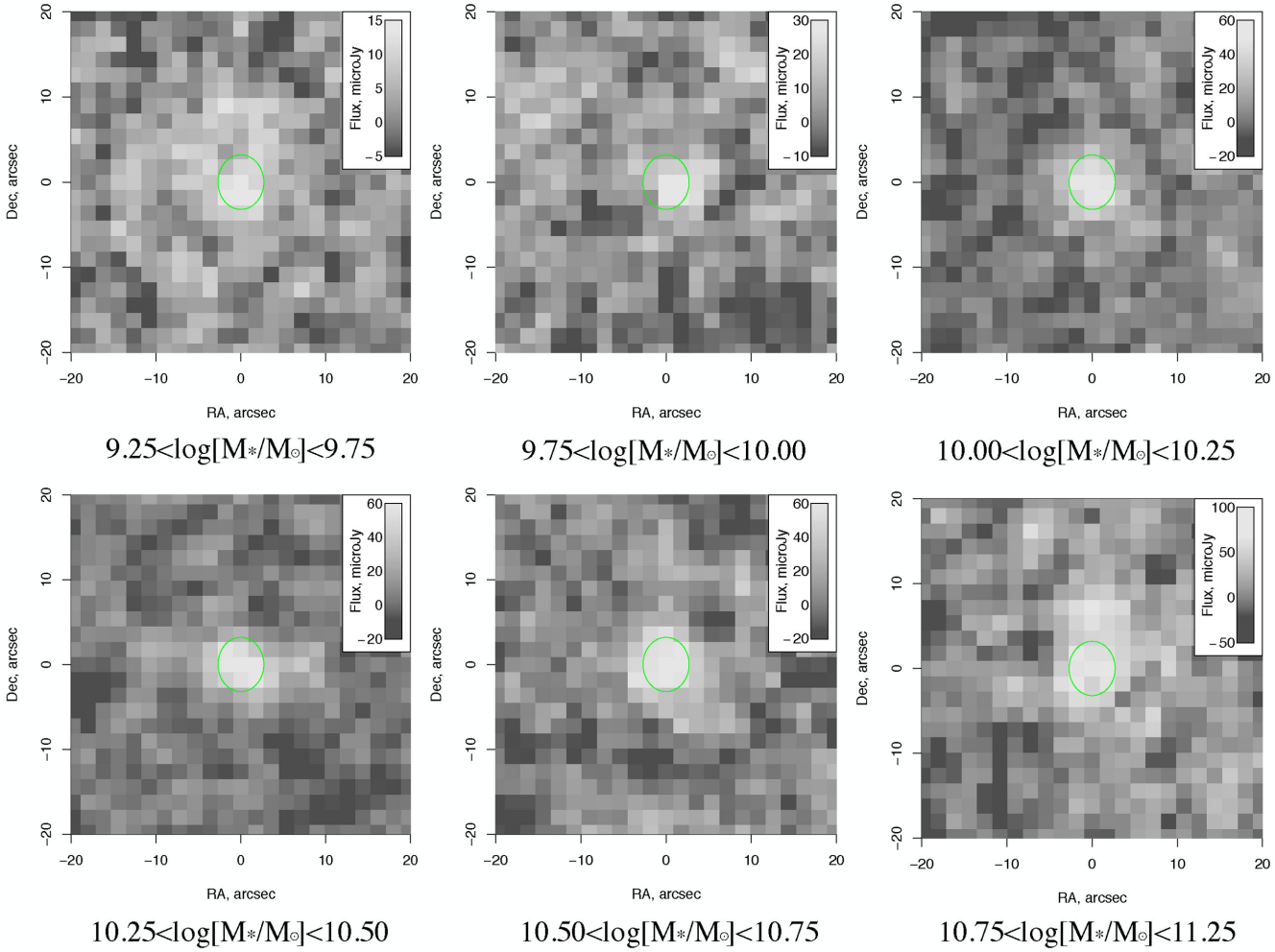

Figure 4. Stacked 1.4 GHz images of our volume-limited late-type sample. The green ellipse shows the FIRST beam shape, centred on the stack position. We also produce stacks excluding individually detected sources, and those produced when stacking in luminosity space for each sample, but for clarity we do not show them here; see text for details.

factor of 1.4 to account for 'CLEAN' bias (see White et al. 2007, for further details). We obtain a $>4.25\sigma$ detection in all bins in our flux density-measured stacks and $>4.5\sigma$ detections in our luminosity-measured stacks.

4 1.4 GHZ LUMINOSITY–SFR RELATION

Using both the individually detected GAMA–FIRST galaxies and our stacked samples, we investigate the 1.4 GHz luminosity–SFR relation. D16 provides multiple SFR estimates using 12 different methods for deriving SFR and produces consistent measurement of star formation across all methods. Here we only compare to the full SED measures of star formation, UV+TIR (UV+TIR1 in D16) and MAGPHYS (da Cunha et al. 2008). Given the recalibration process in D16, all other GAMA SFR methods will produce similar results to the UV+TIR measurement. We also expect the 1.4 GHz SFRs to be most closely correlated with long duration measures of star formation, as they arise from SNe-driven emission. We opt to use the full SED measurements of star formation over FIR emission only (as has previously been used when calibrating 1.4 GHz via the FIR–radio relation), as the UV+TIR SFR estimation combines the SF information derived in the FIR with that observed in the UV, and as such is likely to produce a more representative measure of the total star formation. We also include the MAGPHYS SFR as it gives an alternative estimate of the SF, essentially using information from the UV+TIR, but derived using a different fitting method. Both SFR measures used here assume a Chabrier IMF.

Briefly, the UV+TIR SFR uses the Brown et al. (2014) spectrophotometrically calibrated library of galaxy spectra to derive UV and TIR luminosities, from the GAMA 21-band photometry outlined in Driver et al. (2016a); using *GALEX*-UV, SDSS-optical, VIKING-NIR, *WISE*-MIR and *Herschel*-ATLAS-FIR data. We follow a Bayesian process, with uniform/uninformative priors on the templates (i.e. each template is assumed to be equally likely). For a particular template, the best-fitting/maximum likelihood value and the formal uncertainty are analytic (through the usual propagation of uncertainties). The posterior for the best-fitting value template is given by marginalizing over the full set of templates. By effectively marginalizing over template number as a nuisance parameter, we fully propagated the errors, including uncertainties due to template ambiguities.

MAGPHYS SFRs use the Bruzual & Charlot (2003) stellar populations with a Chabrier (2003) IMF and assumes an angle-averaged attenuation model of Charlot & Fall (2000). This is combined with

an empirical NIR–FIR model accounting for polycyclic aromatic hydrocarbon (PAH) features and NIR continuum emission, emission from hot dust and emission from thermal dust in equilibrium. The code defines a model library over a wide range of star formation histories, metallicities and dust masses and temperatures, and fits the photometry – forcing energy balance between the observed TIR emission and the obscured flux in the UV-optical. Physical properties (SFR, SFH, metallicity, dust mass, dust temperature) for the galaxy are then estimated from the model fits, giving various percentile ranges for each parameter. Here we use the median $\mathrm{SFR}_{0.1\,\mathrm{Gyr}}$ parameter, which provides an estimate for the SFR averaged over the last 0.1 Gyr. Errors on $\mathrm{SFR}_{\mathrm{MAGPHYS}}$ are estimated from the 16th–84th percentile range of the $\mathrm{SFR}_{0.1\,\mathrm{Gyr}}$ parameter, which encompasses both measurement and fitting errors.

For further details of these SFRs, see the more detailed descriptions in D16. We do not use the favoured radiative transfer-derived SFRs of D16 in this work as we do not have these SFRs for the full GAMA–FIRST sample.

Fig. 3 displays the 1.4 GHz luminosity–SFR relation for both the UV+TIR SFR and MAGPHYS SFRs from D16. Individually detected sources from the GAMA–FIRST sample are displayed as circles while the flux density-measured and luminosity-measured stacks are displayed as filled triangles and open squares, respectively. Both methods for determining the stacked fluxes are found to be within the scatter of the individually detected sources, suggesting that stacking method does not strongly affect our results. We do find that the luminosity-measured stacks produce systematically lower luminosity measurements, which potentially suggests that in using a flux stack and median redshift overpredicts to true luminosity. This may be due to the fact that the sources are not uniformly distributed over the redshift of our stacked sample.

We show previously published relations outlined in Hopkins et al. (2003) (from SDSS–FIRST), Boselli et al. (2015) (from the *Herschel* Reference Survey, *K*-band selected sample) and Condon (1992), as the dark green, purple-dashed and orange solid lines, respectively. The Hopkins et al. (2003) line is plotted as a broken power law to account for the scaling for non-thermal radio continuum emission from dwarf galaxies, applied in their relation. All relations are scaled to a Chabrier IMF using the conversions outlined in Haarsma et al. (2000), for Miller-Scalo to Salpeter, and Driver et al. (2013), for Salpeter to Chabrier.

We then fit the 1.4 GHz luminosity–SFR relation linearly in a number of ways using the multidimensional Markov chain Monte Carlo (MCMC) fitting [R] package HYPERFIT[1] (Robotham & Obreschkow 2015). First, we fit the full distribution using a fixed, $m = 1$, slope (blue line), these fits are almost identical for both the UV+TIR and MAGPHYS SFRs but have an offset normalization from the Hopkins et al. (2003) and Condon (1992) relations. Secondly we fit the distributions with a free slope and normalization (magenta line), these fits have a slightly different slope between the UV+TIR and MAGPHYS SFRs. Interestingly for both the UV+TIR and MAGPHYS SFRs this fit has a similar slope and normalization to the lower 1.4 GHz broken power-law component, for dwarf galaxies, of the Bell (2003) and Hopkins et al. (2003) relation (i.e. the dark green and magenta fits have a similar slope at $L_{1.4\,\mathrm{GHz}} < 6.4 \times 10^{21}$ W Hz^{-1}). Lastly, we fit the distributions using just the flux density-measured stacks (green line).

[1] http://hyperfit.icrar.org/

All fits take the form of

$$\log_{10}[\mathrm{SFR}(\mathrm{M}_\odot\,\mathrm{yr}^{-1})] = m \times \log_{10}[L_{1.4\,\mathrm{GHz}}(\mathrm{W\,Hz}^{-1})] + C \quad (1)$$

with parameters, m and C, given in the figure. Given our free fit (which is the best fit to the full data set), we suggest a new calibration to the 1.4 GHz–SFR relation as

$$\log_{10}[\mathrm{SFR}_{\mathrm{UV+TIR}}] = 0.66 \pm 0.02 \times \log_{10}[L_{1.4}] - 14.02 \pm 0.39, \quad (2)$$

$$\log_{10}[\mathrm{SFR}_{\mathrm{MAGP}}] = 0.75 \pm 0.03 \times \log_{10}[L_{1.4}] - 15.96 \pm 0.58. \quad (3)$$

Interestingly, we find best-fitting relations with sublinear slopes (i.e. $m \neq 1$). Given that thermal radio emission scales linearly with SFR (from fundamental theory of the emission processes), this must mean that the non-thermal component is sublinear. This is consistent with non-calorimetric models of non-thermal emission in galaxy discs (e.g. Niklas & Beck 1997; Bell 2003; Lacki, Thompson & Quataert 2010; Irwin et al. 2013; Basu et al. 2015), where cosmic ray electrons do not lose all of their energy before escaping galaxies and not all of their energy is radiated as synchrotron radio emission. These models predict a $\mathrm{SFR} \propto {L_{1.4}}^{0.73\text{–}0.9}$ relation (consistent slope of our MAGPHYS fits). However, the somewhat extreme non-calorimetric models are seemingly in conflict with the tightness of the FIR–radio relation over a broad range of physical properties of the host galaxy (e.g. see discussion in Lacki et al. 2010). While linear, calorimetric, fits ($m = 1$, blue lines) are not in strong conflict with our data (specifically for the MAGPHYS relations), non-calorimetric models for radio emission will require further investigation in the MeerKAT/ASKAP/SKA era.

5 THE 1.4 GHZ SFR–M_* RELATION

Using the 1.4 GHz luminosity–SFR calibration derived above, it is possible to explore the 1.4 GHz SFR–M_* relation (Fig. 5). We display the flux-measured stacked data points as solid black triangles, luminosity-measured stacked data points as open squares and the individually detected GAMA–FIRST sample are shown as circles colour coded by their redshift. We show the SFR–M_* relation fit for the GAMA–SPIRALS sample using the radiative transfer SFRs from D16 as the black solid line, and the same fit at various redshifts (colour coded in the same manner as the data points) using the evolution of the normalization of the SFR–M_* relation using equation (20) of D16. Green dashed and dotted lines show the Hα-derived SFR–M_* fits from SDSS at $z = 0$ (Elbaz et al. 2007) and GAMA I+SDSS at $z < 0.1$ (Lara-López et al. 2013), respectively. These do not include the turnover at high stellar masses as they are fit linearly.

We find that the slope and normalization of the 1.4 GHz SFR–M_* relation from our stacked samples, using our new calibration (black triangles), has the same slope to that derived in D16 at $\log[M_*/\mathrm{M}_\odot] < 10.5$ (Fig. 5); the black line in this figure is the fit using the same sample that is stacked in this work, but with slight normalization offset (∼0.05 dex for the flux-weighted stacks using UV+TIR). While the MAGPHYS stacked data points are ∼0.3 dex lower than the D16 relation, this is roughly consistent with the offset in normalization between the UV+TIR and MAGPHYS SFR–M_* relations in fig. 8 of D16.

The slope of the 1.4 GHz SFR–M_* relation flattens at $\log[M_*/\mathrm{M}_\odot] > 10.5$. This is expected, given the well-known turnover in the SFR–M_* relation at high stellar masses (see Whitaker

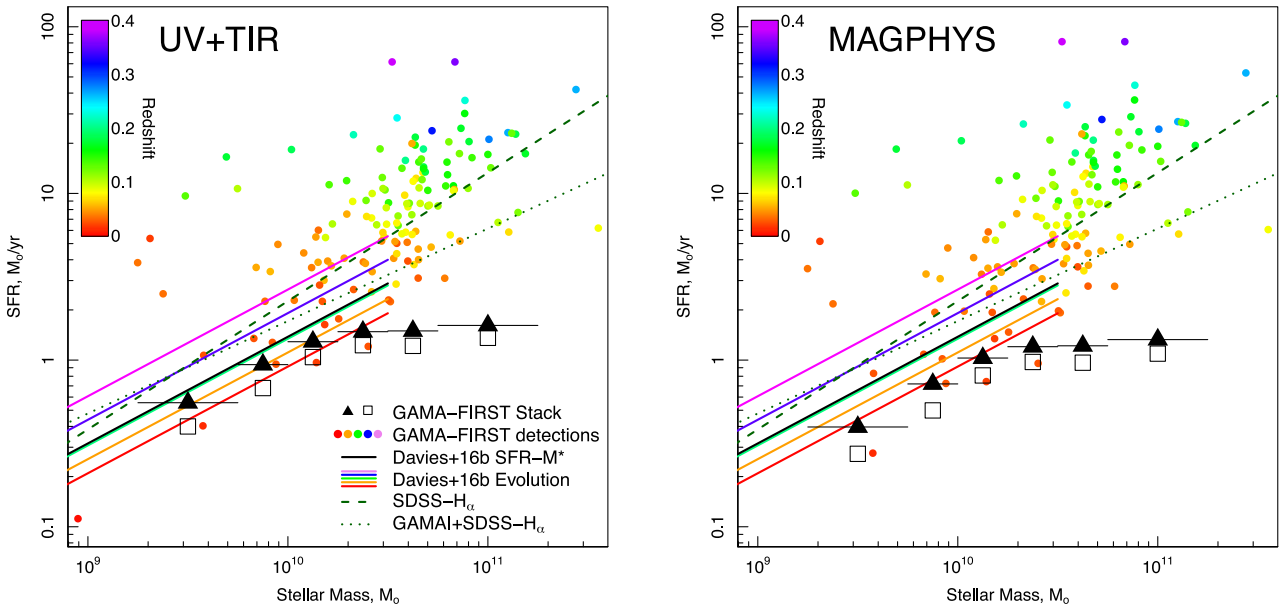

Figure 5. The 1.4 GHz SFR–M_* relation in the GAMA regions, derived using our free-fit luminosity-to-SFR relation for UV+TIR (left) and MAGPHYS (right). Our new 1.4 GHz-derived SFR–M_* relation is consistent with the SFR–M_* relation from Davies et al. (2016) at $\log[M_*/\mathrm{M}_\odot] < 10.5$, but turns over at the high-mass end (the known turnover in the SFR–M_* relation at high stellar mass). Black triangles and open squares display our flux-measured and luminosity-measured stacked samples, respectively, with error bar showing the stacked sample range in stellar mass. Coloured points show the GAMA–FIRST matched sample colour coded by redshift. We also show the SFR–M_* fit from Davies et al. (2016) scaled to various redshifts, given the normalization evolution taken from equation (20) of D16 and colour coded on the same redshift scale as the data points. The black line displays the direct SFR–M_* fit from D16 to an identical sample used in our stacking analysis here. Consequently, the stacked data points should be directly compared to the black line. We also show the Hα-derived SFR–M_* fits from SDSS at $z = 0$ (Elbaz et al. 2007) and GAMA I+SDSS at $z < 0.1$ (Lara-López et al. 2013) as the green dashed and dotted lines, respectively. Errors in median SFR (including fitting errors) are smaller than the symbols.

et al. 2014; Gavazzi et al. 2015; Johnston et al. 2015; Lee et al. 2015; Schreiber et al. 2015; Tomczak et al. 2016, and discussion in D16). The turnover observed here is severe however, given that our stacked sample is based on purely spiral galaxies. We do highlight that there is a turnover observed in other SFR indicators using the same sample (see coloured circles in fig. 8 of D16), but this is less extreme (although only measured to $\log[M_*/\mathrm{M}_\odot] = 10.5$). Potentially we are simply observing the increasing contribution of passive bulges, in terms of specific SFR, in galaxies at the high-mass end. Further studies into the high-mass turnover in comparison to galaxy morphology and components will be the subject of upcoming work (Davies et al., in preparation).

Primarily the GAMA–FIRST individually detected galaxies lie well above the SFR–M_* relation at their redshift, suggesting they are star-bursting galaxies. This is unsurprising, given that they are detected in the relatively shallow FIRST data. The exceptions to this are the very local galaxies (red points), which are mostly consistent with the SFR–M_* relation; very nearby sources can be detected by FIRST to lower SFRs.

It is also interesting to note that using the individually detected GAMA–FIRST galaxies, one would not have been able to define the 1.4 GHz SFR–M_* relation given the small number of sources spread over a large redshift range. This highlights the power in performing optically motivated source stacking of radio continuum data using surveys such as GAMA. The stacked data points allow us explore the 1.4 GHz SFR–M_* relation with lower stellar masses than those probed by the individual detected sources and for the first time, show that the slope and normalization of the 1.4 GHz SFR–M_* relation over 2 decades in stellar mass is consistent with previous estimates using other multiple SFR tracers.

6 PREDICTIONS FOR GAMA–ASKAP

Despite the recent advancements in studying 1.4 GHz emission from galaxies in large area surveys, the relatively shallow depth of current radio continuum surveys such as FIRST and NVSS, and the small area of deep radio continuum surveys, such as VLA-COSMOS (Schinnerer et al. 2007) and ATLAS 1.4 GHz (Hales et al. 2014), have limited the number of sources with detectable 1.4 GHz continuum emission with which to derive SFRs. This is set to change dramatically with the advent of new deep large area continuum surveys from the SKA and its precursors such as ASKAP-EMU (Norris et al. 2011) and MeerKAT-MIGHTEE (Jarvis 2012). One of the key scientific goals of the SKA is to measure the cosmic star formation history using the radio continuum as a dust-unbiased tracer of star formation (see Ciliegi & Bardelli 2015; Jarvis et al. 2015a,b).

A potential limiting factor in the use of the 1.4 GHz SFR tracer in large area surveys, however, is the lack of robust spectroscopic redshifts, with which to derive 1.4 GHz luminosities from observed flux densities and aid in the separation of AGN/SF-like sources. EMU is likely to detect 70 million galaxies, of which only a small faction will have spectroscopic redshifts, mostly at low-z ($z < 0.25$) from EMUs sibling H I spectral line survey WALLABY (see Koribalski 2012) and the local galaxy redshift survey, Taipan. Beyond the very local Universe, EMU will have to either rely on photometric redshifts, undertake additional spectroscopic observations, or use redshifts from existing large area surveys.

The GAMA survey and upcoming Wide Area VISTA Survey (WAVES; Driver et al. 2016b) are ideally suited to providing a large number of spectroscopic redshifts. GAMA contains redshifts for ∼280 000 galaxies in the EMU footprint at $z < 0.4$. In addition, GAMA provides an extensive data base of multiwavelength

observations and value-added catalogues of FIR luminosities, stellar masses, dust masses, metallicities, environmental metrics and most importantly, multiple metrics of star formation with which to compare the observed EMU luminosities (see D16). The upcoming WAVES survey will add ∼2 M galaxies to this sample to $z < 0.8$, which will be invaluable in providing redshifts, environmental metrics and derived parameters for EMU sources. The combination of GAMA/WAVES with the ASKAP surveys (EMU, WALLABY and Deep Investigations of Neutral Gas Origins, DINGO; Meyer 2009) will produce a formidable data set with which to study galaxy evolution over an extensive redshift baseline.

Using the 1.4 GHz luminosity to SFR relations derived in the previous section, we make predictions for the number of GAMA star-forming galaxies that are likely to be detected in upcoming deep radio continuum surveys using ASKAP.

We take the full GAMA $\mathrm{II_{Eq}}$ SFRs derived in D16 for a number of different SFR methods, and use the 1.4 GHz luminosity to SFR relation to predict the rest-frame 1.4 GHz luminosity for all GAMA $\mathrm{II_{Eq}}$ sources. Assuming $\alpha = -0.7$ and the GAMA redshift, we then convert each luminosity to a predicted observed flux density. We then exclude all sources which are detected as an AGN using the BPT diagnostic or have *WISE* colours consistent with an AGN ($\mathrm{W1} - \mathrm{W2} > 0.125$ – as in the top two panels of Fig. 2). We also exclude all sources which do not have a $>2\sigma$ detection in the observable used to determine the source's SFR; such sources may have erroneous measurements of star formation. For MAGPHYS, we only consider sources where the derived SFR is greater than twice the error.

Fig. 6 displays the predicted distribution of 1.4 GHz flux densities from all GAMA $\mathrm{II_{Eq}}$ sources using four of the different SFR methods discussed in D16, for both UV+TIR (top) and MAGPHYS (bottom) calibrations. Hα, u band and UV+TIR SFRs are all derived using the recalibration process detailed in D16. The various histograms in each figure highlight different predictions for the 1.4 GHz flux density distribution from GAMA sources, assuming different SFR measures in GAMA (i.e. how does the choice of SFR tracer in GAMA affect the prediction), while the two sets of panels show the variation based on the 1.4 GHz to SFR calibration used (either equation 2, using UV+TIR, or equation 3, using MAGPHYS). A potential caveat of this analysis is that the 1.4 GHz calibration derived in this work is for late-type star-forming galaxies, but this calibration is applied to all GAMA galaxies (and may not be appropriate in all cases).

We compare this predicted distribution to the observed number density of sources in deep radio continuum surveys, using a combination of the VLA-COSMOS (Schinnerer et al. 2004) and VLA-ECDFS (Miller et al. 2008) surveys. First, we use the VLA-COSMOS 1.4 GHz catalogue of Schinnerer et al. (2007). In order to produce a representative sample of GAMA-like galaxies, we perform a 3 arcsec position match (to be consistent with our previous matching) of the VLA-COSMOS catalogue to the COSMOS photometric catalogue of Capak et al. (2007) and retain matches which have $r < 19.8$, the GAMA selection limit. We then combine this with the VLA-ECDFS optical counterpart catalogue of Bonzini et al. (2012), once again cut at $r < 19.8$. The gold line in Fig. 6 displays the number density as a function of flux density for $r < 19.8$ sources in the combined VLA-COSMOS+ECDFS. We also include a 16 per cent cosmic variance error (gold band), calculated using the prescription in Driver & Robotham (2010)[2] to account for the small volume coverage of these deep surveys at low-z. However, this process does not account for these deep surveys resolving out flux for low-redshift sources.

In addition, we display the predicted number density of sources from the SKA Simulated Skies ($\mathrm{S^3}$) simulations of extragalactic radio continuum sources ($\mathrm{S^3}$-SEX) outlined in Wilman et al. (2008). To make this comparable to a potential GAMA–FIRST sample, we take all sources from $\mathrm{S^3}$-SEX at $z < 0.4$ and match them to the observed distribution of GAMA sources in K-band magnitude (in the absence of stellar mass in the $\mathrm{S^3}$-SEX catalogues). We take the observed K-band distribution from GAMA and randomly sample from the $\mathrm{S^3}$-SEX simulated sources at $z < 0.4$ to produce the same K-mag number density distribution. While this is not ideal, and should be treated as a very loose prediction for a GAMA-like sample, it aims to produce as close to a GAMA representative sample from $\mathrm{S^3}$-SEX as possible. We show the number density of these $\mathrm{S^3}$-SEX sources as the green line in Fig. 6.

Strikingly the predicted number density using the Hα SFRs in GAMA is very close to the observed distribution from VLA-COSMOS+ECDFS and the predicted distribution from $\mathrm{S^3}$-SEX. This suggests that our predictions are producing a comparable number density of 1.4 GHz sources to the observed distribution at >0.3 mJy. The Hα SFR appears most well correlated with the observed distribution, potentially as both mechanisms probe the central regions of galaxies, particularly when using the high-resolution FIRST imaging. It is also important to remember that this Hα SFR has been previously recalibrated using the radiative transfer-derived SFR in D16.

Using these distributions it is therefore possible to make predictions for the number of GAMA sources which are likely to be detectable in EMU and DINGO continuum. The green and red dashed lines in Fig. 6 show the five times rms limits of EMU and DINGO continuum, taken as 0.05 and 0.025 mJy, respectively. Taking the number density of GAMA sources above the EMU limit and scaling to the full GAMA volume (∼250 $\mathrm{deg^2}$) we obtain the predicted number of GAMA-EMU sources, for each SFR method, given in the top right-hand corner of the figure. We then also predict the number of sources which will be undetected in EMU but detectable in the DINGO-continuum overlap with the GAMA-G23 field (∼50 $\mathrm{deg^2}$). The predictions range from ∼65 000 to ∼115 000 GAMA-ASKAP sources depending on SFR tracer used. This suggests that ∼25–45 per cent of GAMA star-forming galaxies (plus many radio-loud AGN) are likely to be detected in GAMA-EMU.

The large uncertainty in these predictions shows the differences/confusion in deriving SFRs using multiple tracers with different assumptions and sources of error, and once again highlights the need for a robust dust unbiased tracer of star formation. A comparison between the true distribution of star-forming galaxies in GAMA–ASKAP and these predictions will help constrain the robustness of individual SFR tracers.

Clearly, using current surveys to investigate the dust-unbiased evolution of star formation in the local Universe is limited by the depth of large area radio surveys – the GAMA–FIRST sample is heavily constrained by the number of FIRST detections. However, with the advent of the ASKAP surveys we will no longer be constrained by the lack of radio detections, but in fact by the number of robust redshifts available to match to secure radio sources. This highlights the necessity for further deep, wide area spectroscopic surveys such as WAVES. Applying the same prescription as above to the current WAVES mock catalogues, we can predict that ∼500 000 of the ∼2 million WAVES sources are likely to be detected by EMU

[2] See http://cosmocalc.icrar.org/

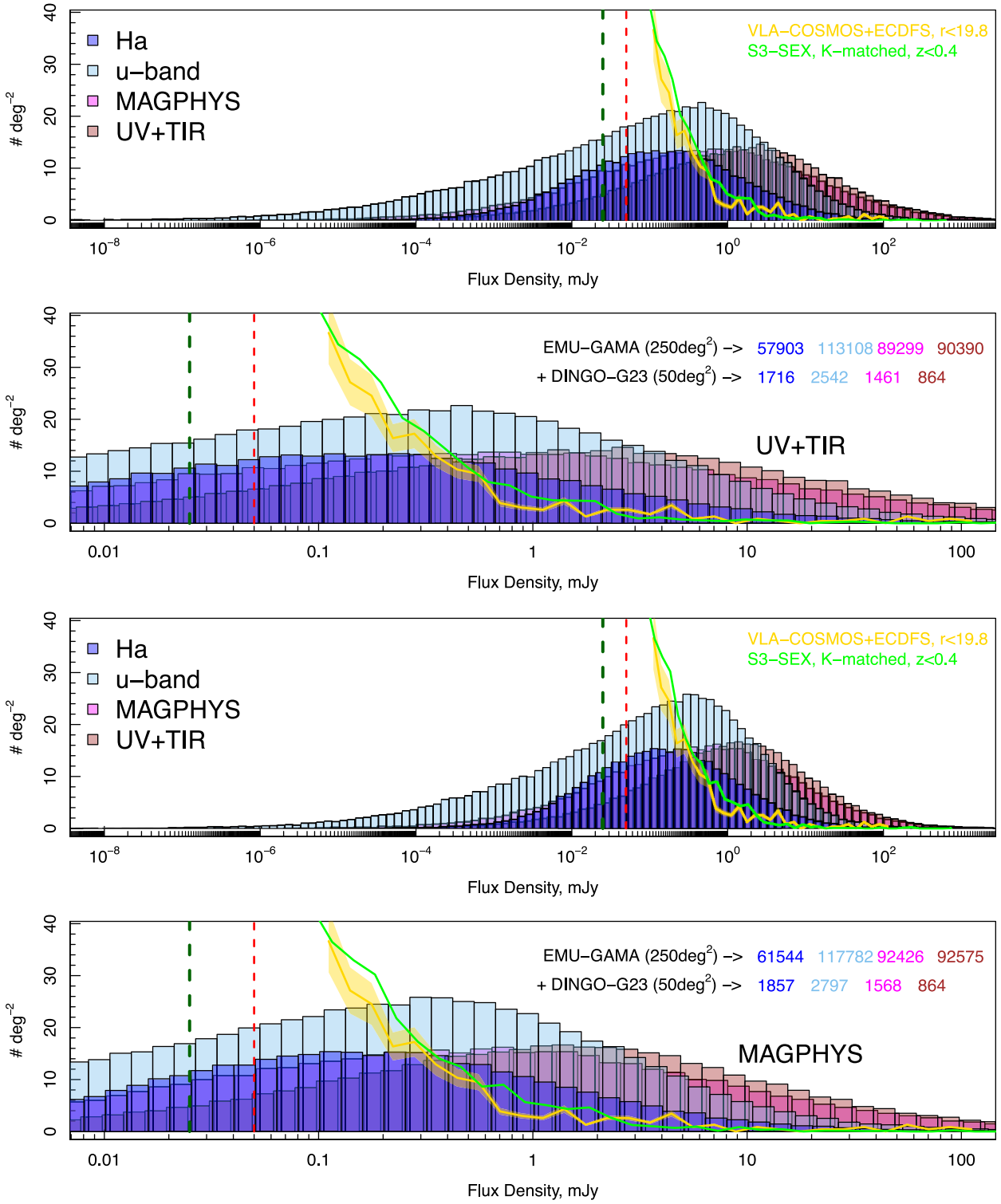

Figure 6. The predicted 1.4 GHz flux density distribution of GAMA star-forming galaxies using different SFR measures. We take the observed SFR from GAMA, convert to a 1.4 GHz luminosity using the UV+TIR (top two panels) and MAGPHYS (bottom two panels) free-fit relation, and scale to an observed flux density using the sources' true redshift. The dashed vertical lines display the ASKAP-EMU (red) and ASKAP-DINGO (green) 1.4 GHz five times rms continuum limits. The top panel shows the full distribution and the bottom panel shows a zoomed in region at the high flux density end. Using these values we can make predictions for the total number of GAMA star-forming galaxies that are likely to be detected in EMU and DINGO (given in the bottom panel for each SFR tracer). The gold line displays the 1.4 GHz number density of r-mag < 19.8 sources from the VLA-COSMOS and VLA-ECDFS surveys, with error band estimated for the 16 per cent cosmic variance error. The green line displays the prediction from a GAMA-like sample in S^3-SEX.

– producing an impressive data set with which to study galaxy evolution from the NUV through to the radio continuum.

7 CONCLUSIONS

We have defined a robust sample of individually detected GAMA–FIRST galaxies and produced a stellar mass weighted stack in the FIRST images at the position of a volume-limited spirals sample in GAMA. We exclude AGN from our sample using the BPT diagram, radio power, *WISE* colours, 1.4 GHz-W4 relation and *r*-band size to produce an uncontaminated star-forming galaxy sample. We then compare the 1.4 GHz luminosity of our sample to previously derived SFRs from GAMA and derive new 1.4 GHz luminosity to SFR calibrations. We derive the dust-unbiased SFR–M_* relation to show that our new calibrations produce a relation with a same slope and normalization roughly consistent to that previously derived for GAMA using 12 other SFR methods (D16), highlighting the power of optically motivated source stacking in large area radio surveys. This also shows that our calibrations are robust in deriving SFRs from radio luminosity. We do find a significant turnover at the high-mass end, potentially highlighting a true turnover in the distribution, which is not observed in D16 (although they do not probe as high in stellar mass).

We use this relation to make predictions for the number of GAMA sources that are likely to be detected in radio continuum by upcoming ASKAP surveys. Using the GAMA Hα SFRs we obtain a prediction which is consistent with existing deep radio surveys at flux density >0.1 mJy. We predict that between 65 000 and 115 000 GAMA sources ($\sim$25–45 per cent) are likely to be detected by ASKAP, and in the near future a further $\sim$500 000 EMU sources will have spectroscopic redshifts from WAVES. The combination of deep, large area radio surveys and spectroscopic redshift surveys will revolutionize our view of dust-unbiased star formation in the Universe.

ACKNOWLEDGEMENTS

GAMA is a joint European–Australasian project based around a spectroscopic campaign using the Anglo-Australian Telescope. The GAMA input catalogue is based on data taken from the Sloan Digital Sky Survey and the UKIRT Infrared Deep Sky Survey. Complementary imaging of the GAMA regions is being obtained by a number of independent survey programs including *GALEX* MIS, VST KiDS, VISTA VIKING, *WISE*, *Herschel*-ATLAS, GMRT and ASKAP providing UV to radio coverage. GAMA is funded by the STFC (UK), the ARC (Australia), the AAO and the participating institutions. The GAMA website is http://www.gama-survey.org/.

REFERENCES

Baldry I. K. et al., 2010, MNRAS, 404, 86
Baldwin J. A., Phillips M. M., Terlevich R., 1981, PASP, 93, 5
Barro G. et al., 2011, ApJS, 193, 30
Basu A., Wadadekar Y., Beelen A., Singh V., Archana K. N., Sirothia S., Ishwara-Chandra C. H., 2015, ApJ, 803, 51
Becker R. H., White R. L., Helfand D. J., 1995, ApJ, 450, 559
Bell E. F., 2003, ApJ, 586, 794
Bell E. F. et al., 2005, ApJ, 625, 23
Bonzini M. et al., 2012, ApJS, 203, 15
Boselli A., Fossati M., Gavazzi G., Ciesla L., Buat V., Boissier S., Hughes T. M., 2015, A&A, 579, A102
Brown M. J. I. et al., 2014, ApJS, 212, 18
Bruzual G., Charlot S., 2003, MNRAS, 344, 1000
Capak P. et al., 2007, ApJS, 172, 99
Chabrier G., 2003, PASP, 115, 763
Charlot S., Fall S. M., 2000, ApJ, 539, 718
Ching J. H. Y. et al., 2017, MNRAS, 464, 1306
Ciliegi P., Bardelli S., 2015, Proc. Sci., Synergistic Science with Euclid and SKA: the Nature and History of Star Formation. SISSA, Trieste, PoS(AASKA14)150
Condon J. J., 1992, ARA&A, 30, 575
Condon J. J., Cotton W. D., Greisen E. W., Yin Q. F., Perley R. A., Taylor G. B., Broderick J. J., 1998, AJ, 115, 1693
Condon J. J., Cotton W. D., Broderick J. J., 2002, AJ, 124, 675
da Cunha E., Charlot S., Elbaz D., 2008, MNRAS, 388, 1595
Davies L. J. M. et al., 2016, MNRAS, in press (D16)
Driver S. P., Robotham A. S. G., 2010, MNRAS, 407, 2131
Driver S. P. et al., 2011, MNRAS, 413, 971
Driver S. P., Robotham A. S. G., Bland-Hawthorn J., Brown M., Hopkins A., Liske J., Phillipps S., Wilkins S., 2013, MNRAS, 430, 2622
Driver S. P. et al., 2016a, MNRAS, 455, 3911
Driver S. P., Davies L. J., Meyer M., Power C., Robotham A. S. G., Baldry I. K., Liske J., Norberg P., 2016b, Astrophys. Space Sci. Proc., 42, 205
Elbaz D. et al., 2007, A&A, 468, 33
Fraser-McKelvie A., Brown M. J. I., Pimbblet K. A., Dolley T., Crossett J. P., Bonne N. J., 2016, MNRAS, 462, L11
Galvin T. J., Seymour N., Filipović M. D., Tothill N. F. H., Marvil J., Drouart G., Symeonidis M., Huynh M. T., 2016, MNRAS, 461, 825
Gavazzi G. et al., 2015, A&A, 580, A116
Gordon Y. A. et al., 2017, MNRAS, 465, 2671
Grootes M. W. et al., 2013, ApJ, 766, 59
Grootes M. W., Tuffs R. J., Popescu C. C., Robotham A. S. G., Seibert M., Kelvin L. S., 2014, MNRAS, 437, 3883
Grootes M. W. et al., 2016, AJ, preprint (arXiv:1612.07322)
Gunawardhana M. L. P. et al., 2013, MNRAS, 433, 2764
Haarsma D. B., Partridge R. B., Windhorst R. A., Richards E. A., 2000, ApJ, 544, 641
Hales C. A. et al., 2014, MNRAS, 441, 2555
Harwit M., Pacini F., 1975, ApJ, 200, L127
Heesen V., Brinks E., Leroy A. K., Heald G., Braun R., Bigiel F., Beck R., 2014, AJ, 147, 103
Helou G., Soifer B. T., Rowan-Robinson M., 1985, ApJ, 298, L7
Hopkins A. M. et al., 2003, ApJ, 599, 971
Hopkins A. M. et al., 2013, MNRAS, 430, 2047
Irwin J. et al., 2013, AJ, 146, 164
Jarvis M. J., 2012, African Skies, 16, 44
Jarvis M. J. et al., 2010, MNRAS, 409, 92
Jarvis M. et al., 2015a, Proc. Sci., The Star-Formation History of the Universe with the SKA. SISSA, Trieste, PoS(AASKA14)068
Jarvis M., Bacon D., Blake C., Brown M., Lindsay S., Raccanelli A., Santos M., Schwarz D. J., 2015b, Proc. Sci., Cosmology with SKA Radio Continuum Surveys. SISSA, Trieste, PoS(AASKA14)018
Johnston R., Vaccari M., Jarvis M., Smith M., Giovannoli E., Häußler B., Prescott M., 2015, MNRAS, 453, 2540
Kauffmann G. et al., 2003, MNRAS, 346, 1055
Kelvin L. S. et al., 2012, MNRAS, 421, 1007
Kennicutt R. C., Evans N. J., 2012, ARA&A, 50, 531
Kennicutt R. C. Jr et al., 2009, ApJ, 703, 1672
Koribalski B. S., 2012, Publ. Astron. Soc. Aust., 29, 359
Lacki B. C., Thompson T. A., Quataert E., 2010, ApJ, 717, 1
Lara-López M. A. et al., 2013, MNRAS, 434, 451
Lee N. et al., 2015, ApJ, 801, 80
Lewis I. J. et al., 2002, MNRAS, 333, 279
Liske J. et al., 2015, MNRAS, 452, 2087
Martin D. C. et al., 2005, ApJ, 619, L1
Mateos S., Alonso-Herrero A., Carrera F. J., Blain A., Severgnini P., Caccianiga A., Ruiz A., 2013, MNRAS, 434, 941
Meurer G. R., Heckman T. M., Calzetti D., 1999, ApJ, 521, 64
Meyer M., 2009, in Heald G., Serra P., eds, Proc. Sci., Exploring the HI Universe with ASKAP. SISSA, Trieste, PoS(PRA2009)015

Miller N. A., Fomalont E. B., Kellermann K. I., Mainieri V., Norman C., Padovani P., Rosati P., Tozzi P., 2008, ApJS, 179, 114
Niklas S., Beck R., 1997, A&A, 320, 54
Noll S., Burgarella D., Giovannoli E., Buat V., Marcillac D., Muñoz-Mateos J. C., 2009, A&A, 507, 1793
Norris R. P. et al., 2011, Publ. Astron. Soc. Aust., 28, 215
Papovich C. et al., 2007, ApJ, 668, 45
Pilbratt G. L. et al., 2010, A&A, 518, L1
Popescu C. C., Tuffs R. J., 2013, MNRAS, 436, 1302
Popescu C. C., Tuffs R. J., Dopita M. A., Fischera J., Kylafis N. D., Madore B. F., 2011, A&A, 527, A109
Rabidoux K., Pisano D. J., Kepley A. A., Johnson K. E., Balser D. S., 2014, ApJ, 780, 19
Robotham A. S. G., Obreschkow D., 2015, Publ. Astron. Soc. Aust., 32, e033
Robotham A. et al., 2010, Publ. Astron. Soc. Aust., 27, 76
Sadler E. M. et al., 2007, MNRAS, 381, 211
Saunders W. et al., 2004, Proc. SPIE, 5492, 389
Schinnerer E. et al., 2004, AJ, 128, 1974
Schinnerer E. et al., 2007, ApJS, 172, 46
Schreiber C. et al., 2015, A&A, 575, A74
Seymour N. et al., 2008, MNRAS, 386, 1695
Sharp R. et al., 2006, Proc. SPIE, 6269, 62690G
Smith D. J. B. et al., 2012, MNRAS, 427, 703
Stern D. et al., 2012, ApJ, 753, 30
Taylor E. N. et al., 2011, MNRAS, 418, 1587
Tomczak A. R. et al., 2016, ApJ, 817, 118
Tuffs R. J., Popescu C. C., Völk H. J., Kylafis N. D., Dopita M. A., 2004, A&A, 419, 821
van der Kruit P. C., 1971, A&A, 15, 110
Whitaker K. E. et al., 2014, ApJ, 795, 104
White R. L., Helfand D. J., Becker R. H., Glikman E., de Vries W., 2007, ApJ, 654, 99
Wilman R. J. et al., 2008, MNRAS, 388, 1335
Wood K., Whitney B. A., Robitaille T., Draine B. T., 2008, ApJ, 688, 1118
Wright A. H. et al., 2016, MNRAS, 460, 765
Yun M. S., Reddy N. A., Condon J. J., 2001, ApJ, 554, 803

This paper has been typeset from a TEX/LATEX file prepared by the author.